

A robust and secure watermarking algorithm based on DWT and SVD in the fractional order fourier transform domain

Ming Tang ^{a,*}, Fuken Zhou ^b

^a Department of Educational Technology, College of Humanities and Education, Foshan University, Foshan, 528000, People's Republic of China

^b Department of Computer Science and Technology, School of Computer, Neusoft Institute Guangdong, Foshan, 528000, People's Republic of China

ARTICLE INFO

Keywords:

Watermarking
Fractional order fourier transform
Singular value decomposition
Discrete wavelet transform

ABSTRACT

The present paper aims to develop and validate a robust and secure watermarking algorithm. Firstly, the algorithm transforms the cover image and the watermark image separately by FRFT to obtain the amplitudes of both the cover image and watermark image, and then the two-level DWT transformation only carries out for the amplitude of the cover image. Secondly, the algorithm applies the SVD to the low-frequency sub-band of the second level DWT of the cover image and the amplitude of the watermark image. Thirdly, a new matrix is constructed based on the singular values from both the cover and watermark images to embed watermark information. Lastly, the algorithm takes the preliminary numerical calculation to determine an appropriate transformation order of FRFT for the cover image and to provide an outstanding balance between the imperceptibility and robustness in the proposed watermarking scheme. Moreover, it guarantees the security of watermarking scheme by the transformation order of FRFT. Experimental results demonstrate that the proposed watermarking scheme provides better performance in imperceptibility and resistance against traditional signal processing and geometric attacks, especially in image rotation, image cropping, average filtering, median filtering, and Gaussian filtering in comparison with the existing methods in the literature.

Credit author statement

Data curation, M.T.; methodology, M.T. and F.K.Zhou; project administration, M.T.; validation, M.T.; Writing-original draft, T.M.; writing-review and editing, M.T., F.K.Zhou. All authors have read and agreed to the published version of the manuscript.

1. Introduction

Digital watermarking is a research topic in modern information security, which involves many research fields such as encryption, digital signal processing, communication technology and multimedia application. The importance of digital watermarking technology in protecting an image from various attacks is highlighted by embedding secret information to a specific host image. With the progress and application of digital multimedia and information technology, the application scopes of digital watermarking have covered information hiding, copyright protection, content integrity authentication, product anti-counterfeiting, product traceability, etc. [1–5] There have been numerous publications over the last 20 years on digital watermarking

technology to meet the growing needs of the information age [6–10]. Based on different application fields, many digital watermarking schemes have been focused and advanced in different perspectives.

It is well known that digital watermarking can be divided into two categories, the spatial domain and the transform domain [11–20]. Most of the previous works on digital watermarking technologies have been conducted in the spatial domain [21–23]. Spatial domain-based transform methods embed watermark information into a host image by directly altering the pixel values of a cover image. The spatial domain-based watermarking schemes have the merits of low complexity and easy implementation, but they are vulnerable to be attacked. The transform domain-based watermarking schemes embed watermark information into a host image by altering the frequency coefficients of an image after various different transformations. In fact, the transform domain-based schemes are mainly based on considerations of both spectral features of images and human visual system to hide the information. At present, the main transformation methods applied to digital watermarking include DCT [15,16,24–27], DWT [28,29] and SVD [30–33] and so on. Most existing schemes in digital watermarking have been proposed based on DCT, SVD, DWT and other technologies in transform domain [6–8,12,17–20,33–36]. The research progress of

* Corresponding author.

E-mail addresses: hunutangming@fosu.edu.cn (M. Tang), zhoufuken@nuit.edu.cn (F. Zhou).

Abbreviations

FRFT	Fractional order Fourier transform
DCT	Discrete cosine transform
DWT	Discrete wavelet transform
SVD	Singular Value Decomposition
PSNR	Peak signal to noise ratio
SSIM	Structural similarity
NC	Normalized correlation
BER	Bit error rate

digital watermarking technologies has been greatly promoted by the aforementioned schemes.

The research field of digital image watermarking has gradually broadened as FRFT domain. FRFT is a new transformation method, which maps information from time (space) axis to frequency axis, and can be rotated by any angle [37]. Compared to the other transformation methods, the watermarking schemes in FRFT domain have offered greater flexibility with regards to the fact that FRFT can simultaneously represent the spatial and frequency information. Tsai et al. [36] embedded watermark information in the domain of FRFT and its four kinds of generalized transforms. Vicente et al. [38] proposed to use the fractional Fourier transform for analyzing and reconstructing the magnetization of the object in the presence of the secondary field. Rawat et al. [39] put forward a robust watermarking algorithm in FRFT domain, where the original image was not altered by embedding the watermark information into the original image. Zhang et al. [40] presented a digital image watermarking technique in FRFT domain and analyzed the energy distribution of the transform image. A chirp typed watermark information was embedded into the spatial domain directly, and detected in the FRFT domain in the paper. Shi et al. [41] designed a novel fractional wavelet transform in order to correct the boundedness of the wavelet and the FRFT. The proposed transform method could provide signal representations in the time-fractional-frequency plane. By analyzing the previous works of literature, these studies have emphasized on watermarking algorithms only in FRFT itself, as opposed to the combination of SVD, DWT and FRFT. These findings suggest that the watermarking schemes only in FRFT domain might not be so effective against different malicious attacks, especially for geometric attacks. There are many alternative methods available for improving the imperceptibility and robustness in a variety of situations. In all of these cases, a robust digital watermarking scheme is proposed based on DWT and SVD in FRFT domain. The proposed watermarking scheme inherits the advantages of multi-resolution analysis of the DWT and the stabilities of SVD as well as the capability of signal representations in FRFT domain. The primary objective of our proposed scheme is to improve the imperceptibility, robustness and security of digital watermarking.

The main focus of this paper is to propose a robust and secure watermarking scheme based on the new blend of DWT and SVD in FRFT domain. It provides an alternative for more secure watermarking embedding technology. In the field of image watermarking based on FRFT, the transformation order of FRFT can be used as a secret key in the process of embedding and extracting watermark information.

The organizational structure of the rest of our paper is as follows. We introduce the fundamental theories in Section 2. Section 3 gives more details of our proposed watermarking scheme. In Section 4, the experimental results and analysis are presented in detail, and the advantages of the proposed scheme compared with other existing schemes are given. Finally, Section 5 summarizes this paper and draws conclusions.

2. Background theory

2.1. Discrete wavelet transform

DWT is an invertible transform in the frequency domain, the working principle of which is based on the wavelets with varying transform frequency. The significance of DWT lies in the ability to decompose signals at different scales, and the selection of different scales can be determined according to different targets. For many signals, the low-frequency component is very important, which often contains the characteristics of the signal, while the high-frequency component gives the details or differences of the signal. Approximation component and detail component are often used in wavelet analysis. Generally speaking, approximation component represents the high-scale of the signal, that is, the low-frequency information; Details component represent the high-scale signal, that is, high-frequency information.

It is a powerful and useful means for signal analyzing and processing, which decomposes a 2D image into four independent sub-bands, namely LL (approximate component details), HL (horizontal component details), LH (vertical component details) and HH (diagonal component details) [5]. An image can be transformed repeatedly by DWT to get multi-scale wavelet decomposition, so as to make it have multiplied approximations and details. The highest coefficient in low-resolution band LL of DWT denotes the most information. The DWT has the characteristics of multi-resolution and multi-layering, and accords with the human vision system. It has certain advantages in improving the imperceptibility of watermark. The formula of DWT can be expressed as follows:

$$W(a, b) = \langle f(t), \psi(a, b) \rangle \quad (1)$$

where a is the scaling factor and b is the translation factor; $f(t)$ represents the specific signal, and $\psi(a, b)$ is the wavelet function. $W(a, b)$ is the result of the wavelet transform, which is a function of a and b .

2.2. Singular value decomposition

SVD, as an effective algebraic feature extraction method in linear algebra, has been widely used in the fields of data dimensionality reduction algorithm, recommendation system, natural language processing and so on. This mainly originates from its good properties, such as good stability. When one image is subject to small disturbance, the singular value of it will not change greatly. In many digital watermarking schemes based on SVD, most watermark information is embedded in a cover image built on a new matrix of singular values.

We study an $m \times n$ matrix A for an image and get the following results by performing SVD on matrix A , as shown in expression (2) [30]:

$$A = U \begin{pmatrix} D & 0 \\ 0 & 0 \end{pmatrix}_{m \times n} V^T \quad (2)$$

where U is a matrix with dimensions $m \times m$ and V^T is a diagonal matrix with dimensions $n \times n$. The columns of U and V^T are referred to as the left and right singular vectors of A , respectively. $D \in R^{r \times r}$ is a square diagonal matrix, $D = \text{diag}(\sigma_1, \sigma_2, \dots, \sigma_r)$ with positive diagonal entries called the singular values of A , which are arranged in descending order: $\sigma_1 \geq \sigma_2 \geq \dots \geq \sigma_r > 0$.

2.3. Fractional order Fourier transform theory and analysis

FRFT is an important method in information analysis and processing for non-stationary signals, which can represent the information in both spatial and frequency domain simultaneously. It is totally different from the conventional Fourier transform that only expresses the information in frequency domain or spatial domain. The two-dimensional fractional order Fourier transform is extended from the one-dimensional fractional order Fourier transform. Suppose that for any two-dimensional signal

$f(s, t)$, the two-dimensional continuous FRFT can be expressed as follows (3) [37]:

$$F^{p1, p2}(u, v) = \int_{-\infty}^{+\infty} \int_{-\infty}^{+\infty} f(s, t) \mathfrak{R}_{p1, p2}(s, t, u, v) ds dt \quad (3)$$

the above two-dimensional FRFT inverse transform can be expressed by the following formula (4):

$$f(s, t) = \int_{-\infty}^{+\infty} \int_{-\infty}^{+\infty} F^{p1, p2}(u, v) \mathfrak{R}_{-p1, -p2}(s, t, u, v) du dv \quad (4)$$

where $\mathfrak{R}_{p1, p2}(s, t, u, v)$ is the kernel function of two-dimensional FRFT $\alpha = p1\pi/2, \beta = p2\pi/2$.

$$\mathfrak{R}_{p1, p2}(s, t, u, v) = \frac{\sqrt{1 - j \cot \alpha} \sqrt{1 - j \cot \beta}}{2\pi} \exp \left[j \left(\frac{s^2 + u^2}{2} \cot \alpha - \frac{su}{\sin \alpha} \right) \right] \exp \left[j \left(\frac{t^2 + v^2}{2} \cot \beta - \frac{tv}{\sin \beta} \right) \right] \quad (5)$$

it is found from the expression (5) that the transform kernel of two-dimensional FRFT can be decomposed into the product of two transform kernels of one-dimensional FRFT, namely:

$$\mathfrak{R}_{p1, p2}(s, t, u, v) = \mathfrak{R}_{p1}(s, u) \times \mathfrak{R}_{p2}(t, v), \quad (6)$$

where $\alpha = \beta = 0$, the two-dimensional FRFT is equal to the function itself; when $\alpha = 0, \beta = \pi/2$, the two-dimensional FRFT is DFT only for t ; when $\alpha = \pi/2, \beta = 0$, the two-dimensional FRFT is DFT only for s ; when $\alpha = \beta = \pi/2$, the two-dimensional FRFT is equivalent to the conventional two-dimensional Fourier transform.

According to formula (3), α and β are the fractional order of the fractional Fourier transform, the rotation angles of the coordinate axes. When the rotation angle α and β is an integer multiple of $\pi/2$, the above fractional Fourier transform becomes the traditional Fourier transform. The traditional Fourier transform is a standard and powerful tool for

analyzing and processing stationary signals, but it is weak for processing and analyzing time-varying non-stationary signals. This is because the traditional Fourier transform uses the global basis function, which highlights the good characteristics of FRFT to analyze some non-stationary signals.

2.4. FRFT of two-dimensional watermark image

Fig. 1(a)-Fig. 1(f) show the FRFT results of the watermark image for Foshan University with different transformation orders. In our paper, we only study the cases of transformation order ($p1 = p2$). As shown in Fig. 1, the information of the two-dimensional watermark image in the spatial-frequency domain is changed with the transformation order of

FRFT. When the transformation order $(p1, p2) = (0, 0)$, the watermark image presents complete spatial domain feature information [Fig. 1(a)]. When the transformation order $(p1, p2) = (1, 1)$, the watermark image presents complete frequency domain feature information [Fig. 1(f)]. The more the transformation order $(p1, p2)$ is close to $(0, 0)$, the more spatial information of the watermark image is reflected in the transformed image after FRFT. The more the transformation order $(p1, p2)$ is close to $(1, 1)$, the more frequency information of the watermark image is reflected in the transformed image after FRFT. In other graphs, the spatial and frequency domain feature components of watermark images are simultaneously included. [Fig. 1(b)-1(e)]. In addition, the watermark images have different transformation coefficients with different transformation orders of FRFT, the transformation coefficients of which corresponds to the ratio of spatial information to frequency information.

It should be noted that the FRFT transform images of the watermark image have certain confidentiality. The original image feature infor-

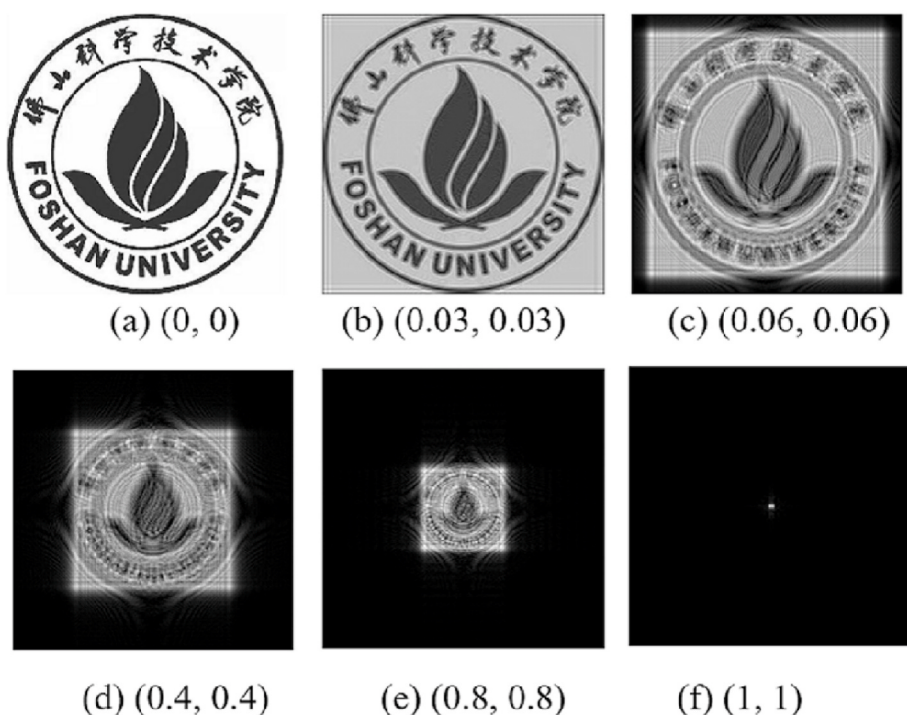


Fig. 1. Two-dimensional image is transformed by FRFT with different transformation orders.

mation can be restored from the transformed image after FRFT with the same transformation order of (p_1, p_2) . If we have no correct transformation order, the original image feature information is not obtained correctly. The transformation order of FRFT (p_1, p_2) can be used as a key for image encryption. Therefore, the proposed scheme based on the combined FRFT and other image watermarking technology will have more freedom, security, and flexibility.

3. A robust watermark embedding and extracting structure based on DWT-SVD in FRFT domain

In this study, a novel image watermarking scheme has been proposed based on DWT-SVD combined technology in FRFT domain. In this section, we comprehensively discuss the proposed watermarking scheme, including the process of watermark embedding and extraction. Suppose I and W indicate the gray cover image with dimension size $M \times M$ and the watermark image with dimension size $L \times L$. I_W represents the watermarked image.

The frame diagram of watermark embedding process is illustrated in Fig. 2. The detailed steps of watermark embedding are given as follows:

Step (1): First, perform FRFT on the cover image I with the transformation order (p_1, p_2) . The amplitude of the cover image after FRFT is obtained, which is implemented by the first level DWT. A low frequency approximation component (LL_1) and three high frequency detail components (HL_1, LH_1, HH_1) of the first layer are generated after the first level of DWT. Next, the low frequency approximation coefficient (LL_1) of the first layer is carried out by the second level DWT to produce a low frequency approximation component (LL_2) and three high frequency detail components (HL_2, LH_2, HH_2) of the second layer. Following that we apply SVD transform to the low frequency approximate coefficient I_F (LL_2) of the second layer and get the singular value S_1 based on the following formula (7).

$$[U_1 S_1 V_1] = SVD(I_F) \quad (7)$$

Step (2): Perform FRFT on the watermark image W with the transformation order (p_1, p_2) . Apply the SVD transform to the amplitude (W_F) of the transformed watermark image after FRFT, and get the corresponding singular value S_2 according to formula (8).

$$[U_2 S_2 V_2] = SVD(W_F) \quad (8)$$

Step (3): Based on the singular values S_1 and S_2 obtained in steps (1) and (2), a new matrix S is constructed according to formula (9) below. Where k is embedding strength. We obtain the low frequency coefficient matrix LL_IW by applying inverse SVD transform to the new matrix S based on Eq. (10).

$$S = S_1 + (S_2 * k) \quad (9)$$

$$LL_IW = U_1 * S * V_1^T \quad (10)$$

Step (4): The low frequency coefficient matrix LL_IW of the above-mentioned image with watermark information features and three detail high frequency coefficients (HL_2, LH_2, HH_2) in step (1) are transformed by the first level DWT inverse transform to obtain the LL_2' matrix coefficient, and then LL_2' matrix coefficient and three high frequency coefficients (HL_1, LH_1, HH_1) are implemented by the second level DWT inverse transform to obtain the low frequency coefficient matrix LL_1' .

Step (5): Perform FRFT inverse transform on LL_1' to form the watermarked image I_W .

The process framework of watermark extraction is illustrated in Fig. 3, and the specific steps of watermark extraction are given as follows:

Step (1): We conduct FRFT on the watermarked image I_W and obtain its amplitude as I_W' .

Step (2): The first level DWT is exerted to the amplitude I_W' and the low frequency approximate component (LL_1) of the first layer is obtained. Then the low frequency approximate component (LL_1) is carried out by the second level DWT. The low frequency approximate coefficient matrix I_F' (LL_2) of the second layer is obtained after the second level DWT transform.

Step (3): The singular value matrix S' is obtained by applying SVD decomposition to I_F' according to formula (11) below. Then the singular value matrix S'_2 corresponding to the watermark information is obtained by the rule of embedding watermark according to formula (12).

$$[U'_2 S' V'_2] = SVD(I_F') \quad (11)$$

$$S'_2 = (S' - S_1)/k \quad (12)$$

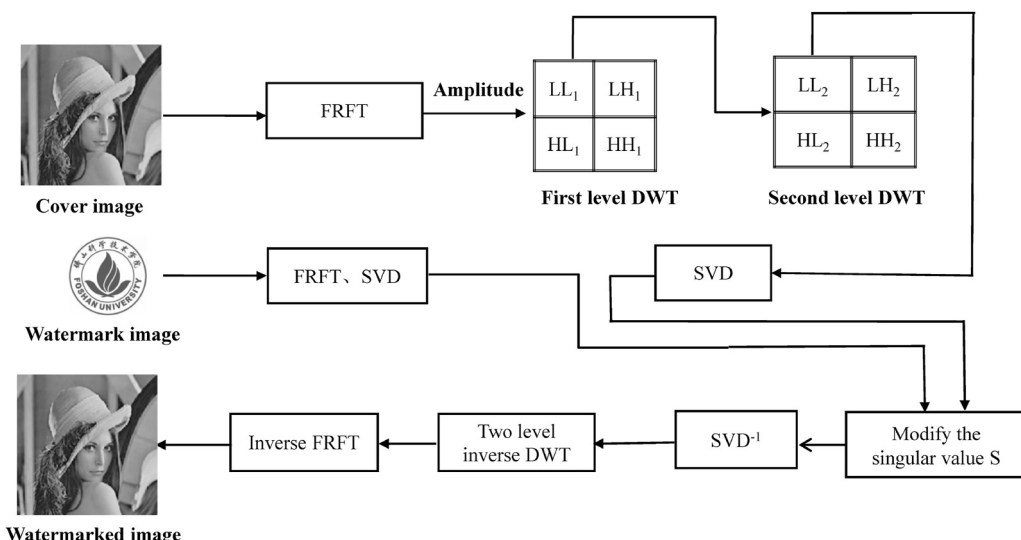


Fig. 2. The process diagram of watermark embedding.

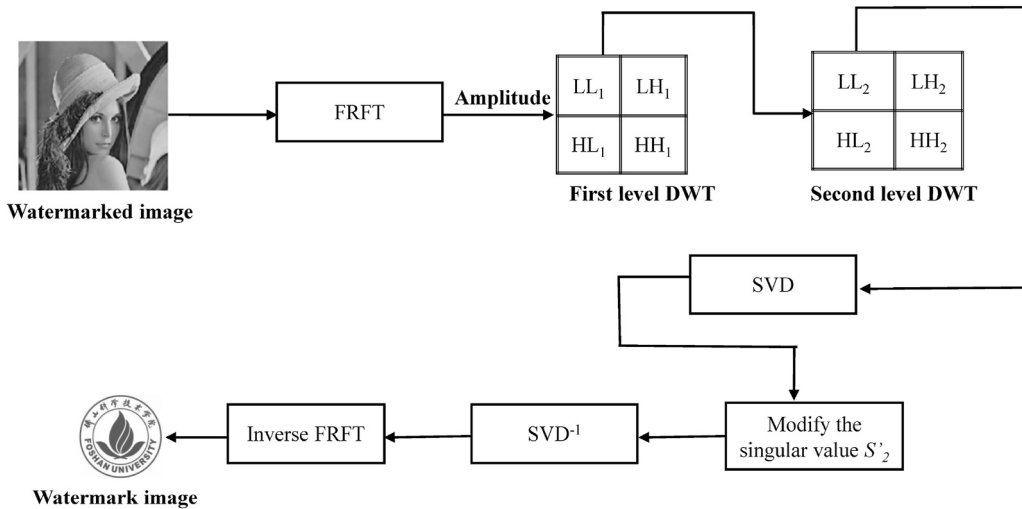


Fig. 3. The process diagram of watermark extracting.

Step (4): For the singular value matrix S'_2 corresponding to the extracted watermark information, we apply the inverse SVD decomposition on S'_2 according to formula (13) and obtain the new matrix W' . Then we use the same transformation order (p_1, p_2) as the watermark embedding and implement inverse FRFT on the W' to obtain the final watermark information.

$$W' = U_2 * S'_2 * V_2^T \quad (13)$$

4. Experiment results and discussions

The cover gray-scale images with the size of 512×512 [Fig. 4(a) - Fig. 4(d)] and the *Foshan University* watermark gray-scale image with the size of 128×128 [Fig. 4(e)] are selected as the simulation objects to analyze and discuss the watermark embedding and extracting mechanism proposed in this paper. All numerical calculations are completed in MATLAB 2019b.

Fig. 4. Cover images (a)-(d) and watermark image for *Foshan University* (e).

where f_{peak} is the peak intensity of original cover image, the value of which is obtained as 255 for the commonly used 8-bit gray-scale image. $f(i,j), g(i,j)$ Denote the gray pixel value of the original cover image and the watermark image corresponding to the location (i,j) . M, N are the width and height of all above images. Generally speaking, the higher the $PSNR$ value, the better the imperceptibility of the image, and the less the image distortion.

$PSNR$ usually ignores the sensitivity of the human visual system, while $SSIM$ [18] reflects the similarity of objects in the scene from image brightness, contrast and structure attributes, which can represent the lack of $PSNR$ to measure the similarity of image structure. Its definition is expressed by the following formula (15):

$$SSIM = [L(f,g)]^\alpha * [C(f,g)]^\beta * [S(f,g)]^\gamma, \quad (15)$$

$$\left\{ \begin{array}{l} L(f,g) = \frac{2\mu_f\mu_g + C_1}{\mu_f^2 + \mu_g^2 + C_1} \\ C(f,g) = \frac{2\sigma_f\sigma_g + C_2}{\sigma_f^2 + \sigma_g^2 + C_2} \\ S(f,g) = \frac{\sigma_{fg} + C_3}{\sigma_f\sigma_g + C_3} \end{array} \right. \quad (16)$$

where three functions $L(f,g), C(f,g), S(f,g)$ denote the comparison functions of brightness, contrast and structure respectively in formula (16). α, β, γ Are parameters that represent the proportion among brightness, contrast and structure. The larger the parameter value, the more important it will be. μ_f, μ_g Denote the mean luminance value of image f and image g respectively, and σ_f, σ_g express the variance of luminance value of image f and image g respectively. σ_{fg} is the covariance between image f and image g . C_1, C_2, C_3 are relatively small constant terms. If $\alpha = \beta = \gamma = 1$ and $C_2 = 2C_3$, $SSIM$ index can be reduced to the following formula (17):

$$SSIM(f,g) = \frac{(2\mu_f\mu_g + C_1)(2\sigma_{fg} + C_2)}{(\mu_f^2 + \mu_g^2 + C_1)(\sigma_f^2 + \sigma_g^2 + C_2)}, \quad (18)$$

The robustness of the algorithm is the ability of the watermarked image to against various attacks, mainly including image processing and geometric transformation. NC and BER between the original watermark and the extracted watermark are two widely common means to estimate the quality of extraction watermark. They measure the difference between the extracted watermark image and the original watermark image. The larger the NC value, the smaller the BER value will be. It indicates the extracted watermark image is more similar to the original watermark image; otherwise, the extracted watermark image is less similar to the original watermark image. The NC is expressed as follows (17):

$$NC = \frac{\sum_{i=1}^{P_W} \sum_{j=1}^{Q_W} [W(i,j) \times W'(i,j)]}{\sqrt{\sum_{i=1}^{P_W} \sum_{j=1}^{Q_W} W^2(i,j)} \sqrt{\sum_{i=1}^{P_W} \sum_{j=1}^{Q_W} W'^2(i,j)}},$$

where W, W' indicate that the original watermark image with the same dimension size of $P_W \times Q_W$ as the extracted watermark. Generally, the range of NC value is $(0, 1)$. The more the value of NC is close to 1, the more similar the two images.

The BER is defined as the ratio of the number of error bits to the total number of bits to measure the accuracy of data transmission. It can be expressed by formula (19) as follows:

$$BER = \frac{1}{P_W \times Q_W} \sum_{i=1}^{P_W} \sum_{j=1}^{Q_W} [W(i,j) \oplus W'(i,j)] \times 100\%, \quad (19)$$

where $W(i,j), W'(i,j)$ represent the original watermark image and the

extracted one with the same dimension size of $P_W \times Q_W$ respectively in formula (19). The symbol \oplus indicates XOR operation. Generally, the smaller the value of BER , the better the robustness of the watermark image.

4.2. The determination of FRFT transformation order

The imperceptibility and robustness are two contradictory criteria for almost all the watermarking schemes. When a watermarking scheme has higher imperceptibility, it has weaker robustness, and vice versa. In the specific evaluation index, the higher the $PSNR$ and $SSIM$, the better the imperceptibility will be. In fact, lower BER and higher NC value means greater watermarking robustness. How to balance the imperceptibility and robustness is the first problem for the further studying of the proposed watermarking scheme in FRFT domain. The transformation order of FRFT must be determined so that the imperceptibility and robustness can be acceptable. We have established the quantitative relationship between FRFT transformation order and $PSNR$, $SSIM$, BER and NC , as shown in Fig. 5(a) to Fig. 5(d). Fig. 5(a) and (b) show the $PSNR$ and $SSIM$ values of embedding watermark information in the original cover image Lena with different FRFT transformation orders. At the same time, the average BER and the average NC of Lena are calculated with FRFT transformation orders against four typical attacks, as shown in Fig. 5(c) and (d). The four typical attacks are Gaussian noise ($m = 0, v = 0.05$), Gaussian filtering ($s = 1$), histogram equalization and rotation attack (rotation angle = 30°). As shown in Fig. 5(a) and (b), the watermarked image has better transparency with the increase of FRFT transformation order. The larger the FRFT transformation order, the larger the overall trend value of $PSNR$ and $SSIM$ values in a certain range will be. As shown in Fig. 5(c) and (d), the average NC decreases with the increasing FRFT transformation order against four typical attacks while the average BER shows up an opposite tendency. It means that the robustness of watermark becomes worse with the increase of FRFT transformation order.

From the results of Fig. 5, it is shown that the range of the appropriate transformation order of FRFT can be determined, to achieve a relative balance between imperceptibility and robustness. When the transformation order of FRFT is in the range of 0–0.1, the $PSNR$ and $SSIM$ values and average NC are relatively high and the average BER is low, so the imperceptibility and robustness are acceptable in this appropriate range of transformation order of FRFT.

4.3. The analysis and discussion of imperceptibility

In this subsection, we select four different cover images and embed the watermark into four different cover images to estimate the imperceptibility of our proposed watermarking scheme. The corresponding values of $PSNR$ and $SSIM$ have been calculated in selecting an appropriate FRFT transformation order $p1 = p2 = 0.05$, as described in Table 1. The corresponding values of $PSNR$ and $SSIM$, which are relatively high and stable, are shown in Table 1. The average value of $PSNR$ is 57.53 and the average value of $SSIM$ is 0.885, both of which are at a high level. As we can see in Table 2, the obtained $PSNR$ for the proposed scheme are satisfactory in comparison experiments. It is demonstrated that the proposed watermarking scheme in our paper meets the requirements of the imperceptibility of cover images.

4.4. The analysis and discussion of robustness in digital watermarking

In this section, we evaluate the robustness of our proposed watermarking scheme against many typical attacks by calculating BER value and NC value between the original watermark and the extracted one. Generally, typical attacks mainly consist of signal processing and geometric transformation. Signal processing attacks mainly include median filtering, Gaussian filtering, average filtering, Gaussian noise, salt and pepper noise, speckle noise, JPEG compression, histogram equalization,

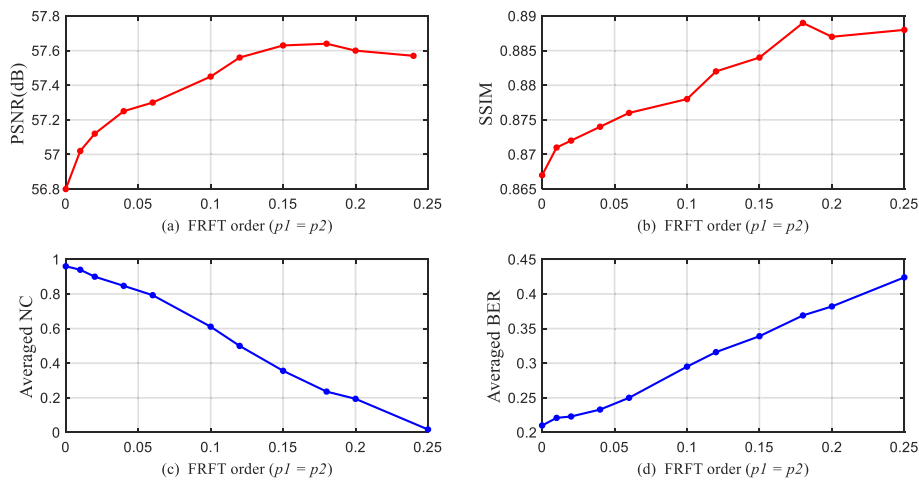


Fig. 5. Relationship between transformation order of FRFT ($p_1 = p_2$) and PSNR, SSIM, NC, BER.

Table 1
Objective evaluation of imperceptibility for four different cover images.

Cover image	PSNR	SSIM
Lena	57.31	0.87
Wom	57.61	0.91
Camera	57.60	0.88
Einstein	57.59	0.88
Average	57.53	0.885

Table 2
Imperceptibility results comparison with related work.

Our	Lai & al [47]	Ganic & al [48]	Zermi [44]	Liu and Tan [30]
PSNR	57.53	50	35	55.85

contrast adjustment, motion blur, etc. Geometric transformations include image cropping, image scaling, rotation attacks, etc. The NC values and BER values are calculated for the four watermarked images, corresponding to the extracted watermark image against the above signal processing and geometric attacks, as shown in [Table 3](#) and [Table 4](#). The majority NC values of the extracted watermark are greater

than 0.98, while the corresponding values of BER are generally less than 0.25. In addition, the cover image Einstein containing the watermark image is attacked against many signal processing and geometric transformations and the watermark are extracted in [Fig. 6](#). [Fig. 6](#) illustrates the visual effect of the watermark extracted against the noise attack is slightly general, while the effect of the extracted watermark is very satisfactory against other image attacks. The above results show our proposed scheme in the paper has strong robustness for typical attacks such as image filtering, rotation attack, scaling attack, salt and pepper noise, image cropping, JPEG compression, histogram equalization, Gaussian noise, speckle noise and so on.

In the field of digital watermark, geometric attacks are often encountered, such as image rotation and image scaling. Many existing schemes are not very strong robustness against geometric attacks [42–44]. We investigate the quality of the extracted watermark against the two geometric attacks. Specifically, the quantitative relationship between the NC and BER values with the rotation angle and size of scale has been established, as shown in [Fig. 7](#) and [Fig. 8](#). As shown in [Fig. 7\(a\)](#) and [\(b\)](#), the NC and BER values change continuously with the rotation angle in range of 0° – 90° . When the rotation angle is greater than 50° , most NC values are more than 0.97, while the BER value is less than 15%. In addition, the larger the rotation angle, the smaller the BER value will be. In the whole range of rotation angle, the values of NC and BER

Table 3
Image processing and geometric attacks (1).

Attack type	Einstein		Lena		Wom		Cameraman	
	NC	BER	NC	BER	NC	BER	NC	BER
Gaussian filtering (3×3)	0.990	0.057	0.992	0.058	0.991	0.063	0.991	0.065
Gaussian filtering (5×5)	0.992	0.070	0.992	0.059	0.991	0.063	0.991	0.065
Gaussian filtering (9×9)	0.992	0.058	0.992	0.059	0.991	0.063	0.991	0.065
Median filtering (3×3)	0.990	0.064	0.991	0.066	0.988	0.072	0.989	0.074
Median filtering (5×5)	0.987	0.074	0.988	0.075	0.985	0.082	0.984	0.083
Average filtering (3×3)	0.989	0.068	0.990	0.069	0.988	0.074	0.987	0.078
Average filtering (5×5)	0.984	0.084	0.985	0.084	0.981	0.089	0.979	0.098
JPEG compression ($Q = 30$)	0.984	0.101	0.981	0.112	0.965	0.159	0.973	0.238
JPEG compression ($Q = 60$)	0.938	0.242	0.848	0.380	0.932	0.218	0.703	0.567
JPEG compression ($Q = 90$)	0.865	0.245	0.865	0.271	0.920	0.237	0.855	0.279
Contrast adjustment	0.954	0.563	0.958	0.624	0.635	0.716	0.945	0.589
Histogram equalization	0.984	0.215	0.981	0.215	0.987	0.215	0.988	0.215
Rotation attacks 30°	0.953	0.136	0.956	0.219	0.954	0.145	0.925	0.244
Rotation attacks 60°	0.967	0.128	0.968	0.216	0.976	0.121	0.872	0.025
Rotation attacks 90°	0.992	0.059	0.991	0.062	0.989	0.067	0.989	0.072
Image cropping 25%	0.970	0.125	0.979	0.532	0.991	0.063	0.941	0.182
Image cropping 50%	0.875	0.289	0.916	0.262	0.941	0.223	0.877	0.278
Image scaling 0.5	0.910	0.660	0.948	0.643	0.958	0.588	0.872	0.660
Image scaling 1.2	0.980	0.099	0.987	0.072	0.985	0.119	0.986	0.216
Image scaling 1.5	0.969	0.105	0.970	0.098	0.970	0.182	0.986	0.119

Table 4

Image processing and geometric attacks (2).

Attack type	Einstein		Lena		Wom		Cameraman	
	NC	BER	NC	BER	NC	BER	NC	BER
Gaussian noise ($m = 0, v = 0.01$)	0.800	0.215	0.804	0.215	0.808	0.215	0.797	0.215
Gaussian noise ($m = 0, v = 0.05$)	0.827	0.214	0.825	0.215	0.828	0.215	0.828	0.215
Salt and pepper noise ($d = 0.01$)	0.883	0.213	0.886	0.213	0.887	0.213	0.884	0.213
Salt and pepper noise ($d = 0.05$)	0.891	0.215	0.890	0.215	0.890	0.215	0.888	0.214
Salt and pepper noise ($d = 0.4$)	0.801	0.215	0.811	0.215	0.810	0.215	0.807	0.215
Speckle noise ($v = 0.2$)	0.866	0.236	0.849	0.259	0.911	0.232	0.831	0.270
Speckle noise ($v = 0.6$)	0.879	0.226	0.867	0.245	0.922	0.219	0.838	0.250

**Fig. 6.** Einstein embedded with watermark image and the extracted watermarks against different attacks.

are relatively good and acceptable. Fig. 8(a) and (b) illustrate that the NC values and BER values change with the size of scale against image scaling attacks. Here, we explore the case the size of scale is 0.5–2.5. When the size of scale is less than 1.5, the NC values is greater than 0.98, and the BER values is also within the acceptable range. It is demonstrated that our proposed watermarking scheme in this paper has strong robustness in anti-rotation attack and anti-scaling attack.

We calculate the NC values of Lena cover image against image processing, and compare them with other schemes, which are shown in Table 5 [19,36,46]. These image processing attacks include Gaussian filter ($3 \times 3, 5 \times 5$), median filter ($3 \times 3, 5 \times 5$), Gaussian noise ($m = 0, v = 0.03$), pepper and salt noise ($d = 0.02$), average filtering (3×3) and histogram equalization. As shown in Table 4, the NC values of our proposed scheme are almost in the high range, which are slightly lower than those of Ernawan [36] for Gaussian filter (5×5) and median filter (3×3). The values of NC in our proposed scheme are higher than those of NC corresponding to Liu [19] except the Pepper and salt noise ($d =$

0.02) and corresponding to Zhou [46] except the Gaussian noise ($m = 0, v = 0.03$) and Pepper and salt noise ($d = 0.02$). More importantly, our proposed scheme has more obvious and outstanding advantages in anti-geometric attacks. We also calculate the values of NC against geometric attacks and compare them with the other watermarking schemes. Fig. 9 shows the NC values of the extracted watermark image using different schemes [42–45]. In terms of image rotation and image cropping, the NC values of the proposed scheme in this paper are greater than those of the other four schemes [42–45], indicating its great advantages. In the aspect of image scaling, the NC values of our proposed scheme are slightly larger than those of Jimson [42] and Zear [43], but much larger than those of the other two schemes.

From the experimental comparison results in Figs. 5–9 and Tables 1–5, it is proved that our proposed scheme based on DWT and SVD in FRFT domain provides greater imperceptibility and robustness. It has good imperceptibility and robustness for the following reasons: (1) We make use of FRFT with the ability to express the information characteristics in

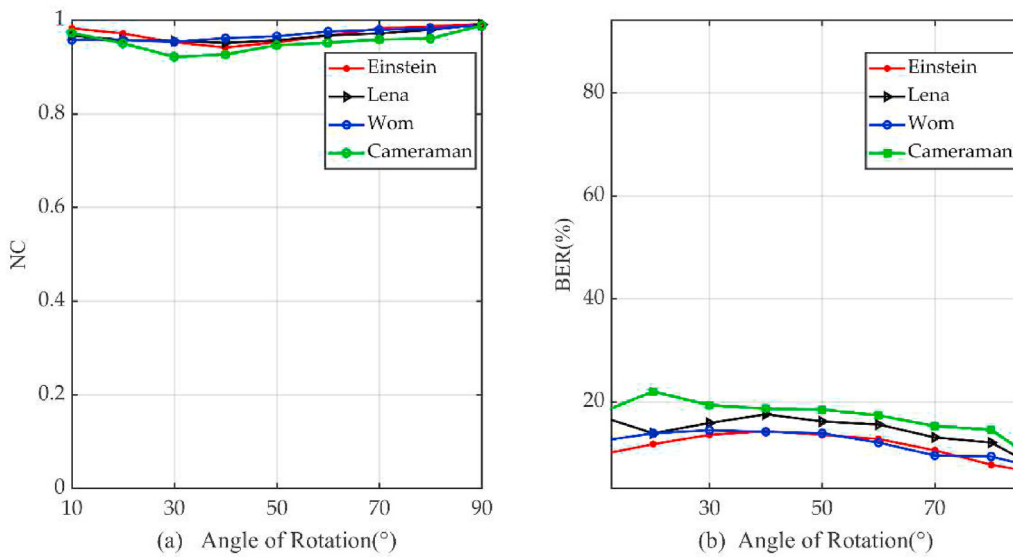


Fig. 7. NC and BER values of the extracted watermark with different angles against rotation attacks.

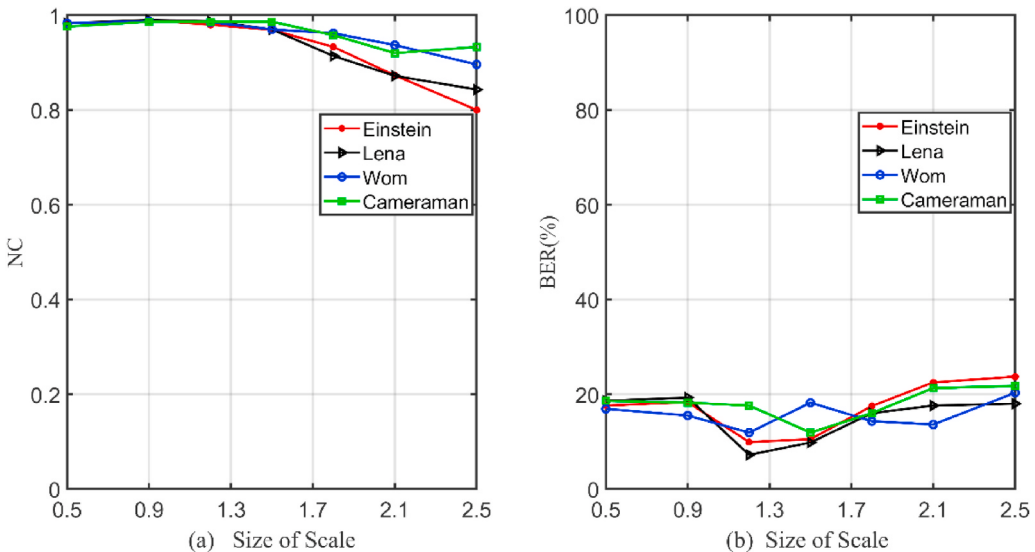


Fig. 8. NC and BER values of the extracted watermark with different sizes against scaling attacks.

Table 5

Comparison of NC values for the several schemes against different image processing.

Attack type	Liu et al. [19]	Ernawan et al. [36]	Zhou et al. [46]	Proposed
Gaussian filtering (3×3)	0.975	0.987	0.963	0.992
Gaussian filtering (5×5)	0.967	0.999	0.935	0.992
Median filtering (3×3)	0.969	0.999	0.979	0.991
Median filtering (5×5)	0.945	0.710	0.972	0.988
Gaussian noise ($m = 0$, $v = 0.03$)	0.802	0.725	0.998	0.825
Pepper and salt noise ($d = 0.02$)	0.998	0.880	0.972	0.893
Average filtering (3×3)	0.953	0.809	0.974	0.990
Histogram equalization	0.987	—	0.857	0.981
JPEG compression	0.968	0.923	0.931	0.978

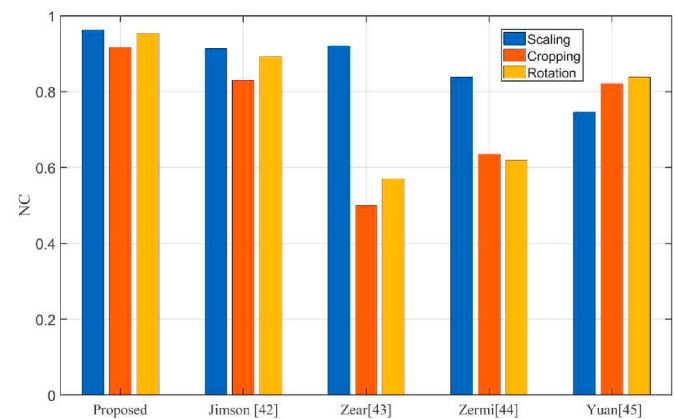


Fig. 9. Comparison of NC values of the extracted watermarks by different watermarking schemes against geometric attacks ([42] Jimson et al., 2018 [43]; Zear et al., 2018 [44]; Zermi et al., 2021 [45]; Yuan et al., 2019).

spatial and transform domain simultaneously; (2) We have the advantages of both spatial and transform domain in watermarking algorithm, combining the multi-resolution features of DWT with the stability of SVD; (3) The transformation order of FRFT is used as a key in the process of extracting watermark, which can make the proposed scheme more secure.

5. Conclusion

To improve the imperceptibility and robustness in invisible watermarking systems, we propose a robust and secure algorithm based on DWT and SVD transform in FRFT domain in this paper. In the preliminary experiment, an appropriate transformation order of FRFT is determined to offer a better balance between imperceptibility and robustness. In addition, the original cover image and watermark image are transformed by FRFT with regards to the fact that FRFT has the ability to simultaneously represent the information in spatial domain and transform domain. Furthermore, in DWT transform, the LL (low frequency component) sub-band, which has the largest energy, is selected to embed the watermark information that improves the robustness against malicious attacks. Then, the watermark embedding is implemented in SVD decomposition by adding the singular values of the original cover image with the singular values of the watermark image multiplied by a scaling factor. Besides, the safety of watermarking scheme is improved by utilizing the transformation order of FRFT. Moreover, the proposed watermarking scheme is based on DWT and SVD transforms in FRFT, which can protect the useful and informative image against various of different extreme signal processing and geometric attacks. The above experimental results confirm that our proposed scheme provides greater visual imperceptibility and robustness, especially in terms of image rotation, image cropping, average filtering, median filtering and Gaussian filtering compared to other literature schemes. In future, the authors are interested in seeking a new robust image watermarking scheme invariant to extreme signal attacks, such as speckle noise and pepper and salt noise in future communications.

Availability of data and materials

Algorithmic data sharing is not applicable to this paper because no datasets were generated or analyzed in this study.

Declaration of competing interest

The authors declare that they have no known competing financial interests or personal relationships that could have appeared to influence the work reported in this paper.

Acknowledgements

We would like to acknowledge our sincere thanks to the Management of our Colleges, our Colleagues of Foshan University.

References

- [1] Dashti MT, Mauw S. Handb Financ Cryptogr Secur 2010;109–32.
- [2] Niu XM, Lu ZM, Sun SH, S H. Digital watermarking of still images with gray-level digital watermarks. *IEEE Trans Consum Electron* 2000;46:137.
- [3] Hsu CT, Wu JL. Hidden digital watermarks in images. *IEEE Trans Image Process* 1999;8:58.
- [4] Shieh CS, Huang HC, Wang FH, Pan JS. Genetic watermarking based on transform-domain techniques. *Pattern Recogn* 2004;37:555.
- [5] Mallat SG. A theory for multiresolution signal decomposition: the wavelet representation. *IEEE Trans Pattern Anal Mach Intell* 1989;11:674.
- [6] Ariamanto D, Ernawan F. An improved robust image watermarking by using different embedding strengths. *Multimed Tool Appl* 2020;79:12041.
- [7] Thanki RM, Kothari AM. Hybrid domain watermarking technique for copyright protection of images using speech watermarks. *J Ambient Intell Hum Comput* 2020;11:1835.
- [8] Fares K, Amine K, Salah E. A robust blind color image watermarking based on Fourier transform domain. *Optik* 2020;208.
- [9] Tsui TK, Zhang XP, Androutsos D. Color image watermarking using multidimensional fourier transforms. *IEEE Trans Inf Forensics Secur* 2008;3:16.
- [10] Verma VS, Jha RK, Ojha A. Digital watermark extraction using support vector machine with principal component analysis based feature reduction. *J Vis Commun Image Represent* 2015;31:75.
- [11] Su Q, Niu Y, Wang G, Jia S, Yue J. Color image blind watermarking scheme based on QR decomposition. *Signal Process* 2014;94:219.
- [12] Singh AK, Dave M, Mohan A. Hybrid technique for robust and imperceptible multiple watermarking using medical images. *Multimed Tool Appl* 2016;75:8381.
- [13] Tao P, Eskicioglu AM. An adaptive method for image recovery in the DFT domain. *J Multimed* 2006;1:36.
- [14] Run RS, Horng SJ, Lai JL, Kao TW, Chen RJ. An improved SVD-based watermarking technique for copyright protection. *Expert Syst Appl* 2012;39:673.
- [15] Patra JC, Phua JE, Bornand C. A novel DCT domain CRT-based watermarking scheme for image authentication surviving JPEG compression. *Digit Signal Process A Rev* J 2010;20:1597.
- [16] Rabie T, Kamel I. Toward optimal embedding capacity for transform domain steganography: a quad-tree adaptive-region approach. *Multimed Tool Appl* 2017;76:8627.
- [17] Singh S, Rathore VS, Singh R. Hybrid NSCT domain multiple watermarking for medical images. *Multimed Tool Appl* 2017;76:3557.
- [18] Wang Z, Bovik AC, Sheikh HR, Simoncelli EP. Image quality assessment: from error visibility to structural similarity. *IEEE Trans Image Process* 2004;13:600.
- [19] Makbol NM, Khoo BE, Rassem TH. Block-based discrete wavelet transform-singular value decomposition image watermarking scheme using human visual system characteristics. *Image Process Let* 2016;10:34.
- [20] Ahmadi SBB, Zhang G, Wei S. Robust and hybrid SVD-based image watermarking schemes: a survey. *Multimed Tool Appl* 2020;79:1075.
- [21] Van Schyndel RG, Tirkel AZ, Osborne CF. A digital watermark. In: Proc. - Int. Conf. Image process. ICIP; 1994. p. 86–90.
- [22] Petrovic R, Tehranchi B, Winograd JM. Digital watermarking security considerations. In: Proc. Multimed. Secur. Work. 2006; 2006. p. 152–7. MM Sec'06.
- [23] Bender W, Gruhl D, Morimoto N, Lu A. Techniques for data hiding. *IBM Syst J* 1996;35:313.
- [24] Abdulrahman AK, Ozturk S. A novel hybrid DCT and DWT based robust watermarking algorithm for color images. *Multimed Tool Appl* 2019;78:17027.
- [25] Lin SD, Shie SC, Guo JY. Improving the robustness of DCT-based image watermarking against JPEG compression. *Comput Stand Interfac* 2010;32:54.
- [26] Parah SA, Sheikh JA, Loan NA, Bhat GM. Robust and blind watermarking technique in DCT domain using inter-block coefficient differencing. *Digit Signal Process A Rev* J 2016;53:11.
- [27] Parah SA, Sheikh JA, Akhoon JA, Loan NA, Bhat GM. Information hiding in edges: a high capacity information hiding technique using hybrid edge detection. *Multimed Tool Appl* 2018;77:185.
- [28] Sharma A, Singh AK, Kumar P. Combining Haar wavelet and Karhunen-Loeve transform for robust and imperceptible data hiding using digital images. *J Intel Syst* 2018;27:91.
- [29] Wang Y, Doherty JF, Van Dyck RE. A wavelet-based watermarking algorithm for ownership verification of digital images. *IEEE Trans Image Process* 2002;11:77.
- [30] Liu R, Tan T. An SVD-based watermarking scheme for protecting rightful ownership. *IEEE Trans Multimed* 2002;4:121.
- [31] Anand A, Singh AK. An improved DWT-SVD domain watermarking for medical information security. *Comput Commun* 2020;152:72.
- [32] Wang S, Meng X, Yin Y, Wang Y, Yang X, Zhang X, Peng X, He W, Dong G, Chen H. Optical image watermarking based on singular value decomposition ghost imaging and lifting wavelet transform. *Opt Laser Eng* 2019;114:76.
- [33] Bagheri Baba Ahmadi S, Zhang G, Wei S, Boukela L. An intelligent and blind image watermarking scheme based on hybrid SVD transforms using human visual system characteristics. *Vis Comput* 2020;3.
- [34] Ernawan F, Ramalingam M, Sadiq AS, Mustaffa Z. An improved imperceptibility and robustness of 4x4 DCT-SVD image watermarking using modified entropy. *J Telecommun Electron Comput Eng* 2017;9:111.
- [35] Kumar Arvind, Agarwal Pragya, Choudhary Ankur. A digital image watermarking technique using cascading of DCT and biorthogonal wavelet transform. In: Proc. Int. Conf. Recent Cogniz. Wirel. Commun. Image process.; 2016. p. 21–9.
- [36] Ernawan F, Kabir MN. A blind watermarking technique using redundant wavelet transform for copyright protection. In: Proc. - 2018 IEEE 14th Int. Colloq. Signal process. Its Appl. CSPA 2018; 2018. p. 221–6.
- [37] Sejdic E, Djurović I, Stanković L. Fractional Fourier transform as a signal processing tool: an overview of recent developments. *Signal Process* 2011;91:1351.
- [38] Parot V, Sing-Long C, Lizama C, Tejos C, Uribe S, Irarrázaval P. Application of the fractional fourier transform to image reconstruction in MRI. *Magn Reson Med* 2012;68:17.
- [39] Rawat S, Raman B. A blind watermarking algorithm based on fractional Fourier transform and visual cryptography. *Signal Process* 2012;92:1480.
- [40] Zhang F, Mu X, Yang S. Multiple-chirp typed blind watermarking algorithm based on fractional fourier transform. In: Proc. 2005 Int. Symp. Intell. Signal process. Commun. Syst. ISPACS 2005; 2005. p. 141–4.
- [41] Shi J, Zhang NT, Liu XP. A novel fractional wavelet transform and its applications. *Sci China Inf Sci* 2012;55:1270.
- [42] Jimson N, Hemachandran K. DFT based coefficient Exchange digital image watermarking. In: Second International Conference on Intelligent Computing and Control systems, Madurai, India; 2018.

- [43] Zear, Singh AK, Kumar P. A proposed secure multiple watermarking technique based on DWT, DCT and SVD for application in medicine. *Multimed Tool Appl* 2018;77:4863–82.
- [44] Zermi N, Khaldi A, Kafi MR, et al. A lossless DWT-SVD domain watermarking for medical information security. *Multimed Tool Appl* 2021;(4).
- [45] Yuan Z, Liu D, Zhang X, et al. New image blind watermarking method based on two-dimensional Discrete Cosine Transform. *Optik - Int J Light Electron Opt* 2019; 204:164152.
- [46] Zhou X, Zhang H, Wang C. A robust image watermarking technique based on DWT, APDCBT, and SVD[J]. *Symmetry* 2018;10(3):77.
- [47] Lai CC. Digital image watermarking using discrete wavelet transform and singular value decomposition[J]. *IEEE Trans Instrum Meas* 2010;59(11):3060–3.
- [48] Ganic E, Eskicioglu AM. Robust DWT-SVD domain image watermarking: embedding data in all frequencies. In: Proc. Workshop multimedia security, Magdeburg, Germany; 2004. p. 166–74.